

Kernel Learning for High-Resolution Time-Frequency Distribution

Lei Jiang, Haijian Zhang, Lei Yu, and Guang Hua

Signal Processing Lab., School of Electronic Information, Wuhan University, China

Abstract—Kernel functions in quadratic time-frequency distributions (TFDs) are viewed as low-pass filters in the ambiguity function (AF) domain to suppress interfering cross-terms (CTs). Traditional kernel design methods are signal-dependent or have manually selected parameters, which impose restrictions on eliminating CTs and achieving high-resolution TFDs. To address this issue, this paper proposes a data-driven kernel learning model directly from Wigner-Ville distribution (WVD) of the noisy signal. Specifically, the proposed kernel learning based TFD (KL-TFD) model consists of several multi-channel learning convolutional kernels stacked to simulate adaptive directional filters, and increasing dilations are adopted to enlarge the kernel size so that a trade-off between computation and performance is achieved. In addition, channel-wise weights are employed to distinguish the significant directions and trivial ones. Finally, channel fusion is implemented by a simple 1×1 convolutional kernel. Numerical experiments examined over both synthetic and real-life data confirm that the proposed KL-TFD provides the state-of-the-art performance when compared to existing kernel function design based methods.

Index Terms—Time-Frequency Distribution, Kernel Learning

I. INTRODUCTION

TIME-FREQUENCY distributions (TFDs) provide a comprehensive description of nonstationary signals [1]–[3] while limited by the issues of time-frequency (TF) resolution, cross-terms (CTs) suppression, spectrally-overlapped components, noise interference, etc. Therefore, a high-resolution TFD to tackle the above issues is of vital importance for plenty of practical applications as most real-life signals are nonstationary [4]–[10]. This paper emphasizes on the high-resolution TF representation of nonstationary signals in different signal-to-noise ratio (SNR) environments.

On the one hand, the wavelet transform (WT) [11], which is regarded as a classical linear TFD, employs adaptive window sizes to improve the TF resolution compared to the commonly-used short-time Fourier transform (STFT). From the perspective of post-processing based on WT or STFT, the reassignment (RS) methods [12] assign the average energy in certain domains to the gravity center of energy distributions to gain instantaneous frequency (IF) trajectories. Furthermore, the synchrosqueezing transform (SST) [13], [14] squeezes the TF coefficients into the IF trajectory only in the frequency direction instead of in both time and frequency directions for RS. Inspired by the SST, the synchroextracting transform (SET) [15] was proposed to generate a more energy concentrated TFD and meanwhile allow for signal reconstruction. Recently, thanks to the simplicity and immunity to CTs of linear TFDs, Abdoush *et al.* [16] proposed an adaptive IF estimation method for noisy multicomponent signals based on

two developed linear TF transforms. However, linear TFDs generally suffer from low TF resolution and signal distortion especially in strong noise situations.

On the other hand, quadratic TFDs with high TF resolution, e.g., Wigner-Ville distribution (WVD) [2], also have difficulty in interpreting the signal in the 2-dimensional (2D) TF plane due to significant CTs [17]. Considerable investigations are therefore dedicated to reducing CTs while preserving high concentration. Particularly, kernel function based TF analysis methods [4] viewed as smoothed versions of the standard WVD have been extensively studied, and they can be roughly divided into two categories: signal-independent TFDs and signal-dependent TFDs. The former kernel function design methods are regarded as low-pass filters since CTs have oscillatory characteristics, e.g., Choi-Williams distribution (CWD) [18] and B-distribution (BD) [19]. Moreover, separable kernel functions which separately smooth along both time and frequency axes are designed to further improve resolution, e.g., S-method (SM) [20], extended modified B-distribution (EMBD) [21], and compact kernel distribution (CKD) [22].

However, the above kernel design methods have fixed or manually selected parameters, which might ignore some crucial information of signal intrinsic characteristics, e.g., the direction of analytic signals. Thus, signal-dependent kernel functions are designed with respect to certain criteria to gain better TF representation, e.g., radially Gaussian kernel (RGK) [23], adaptive optimal-kernel (AOK) [24], [25], adaptive directional TFD (ADTFD) [26], [27], locally optimized ADTFD (LO-ADTFD) [28], multi-directional distribution (MDD) [29]. Specifically, the ADTFD adapts the direction of smoothing kernel at each TF point, as a result of which TF resolution and reduction of CTs can be highly improved. The MDD is specifically designed for piece-wise linear frequency-modulated signals. Although most of signal-dependent kernel methods achieve better performance than signal-independent ones, their kernel optimization is subject to certain criteria and given signal type.

In this paper, motivated by the fact that deep learning techniques are capable of learning TF structure and immune to noise [30], we propose a novel kernel learning based TFD (KL-TFD) directly from WVD. Inspired by the 2D convolution relationship between WVD and smoothed quadratic TFD, a convolutional neural network (CNN) takes place of traditional kernel functions imposed in ambiguity function (AF) plane, and multi-channel learning convolutional kernels are utilized to simulate adaptive directional filters, i.e., each channel controls respective direction. Furthermore, increasing dilation factors are employed to ensure a large kernel size as well

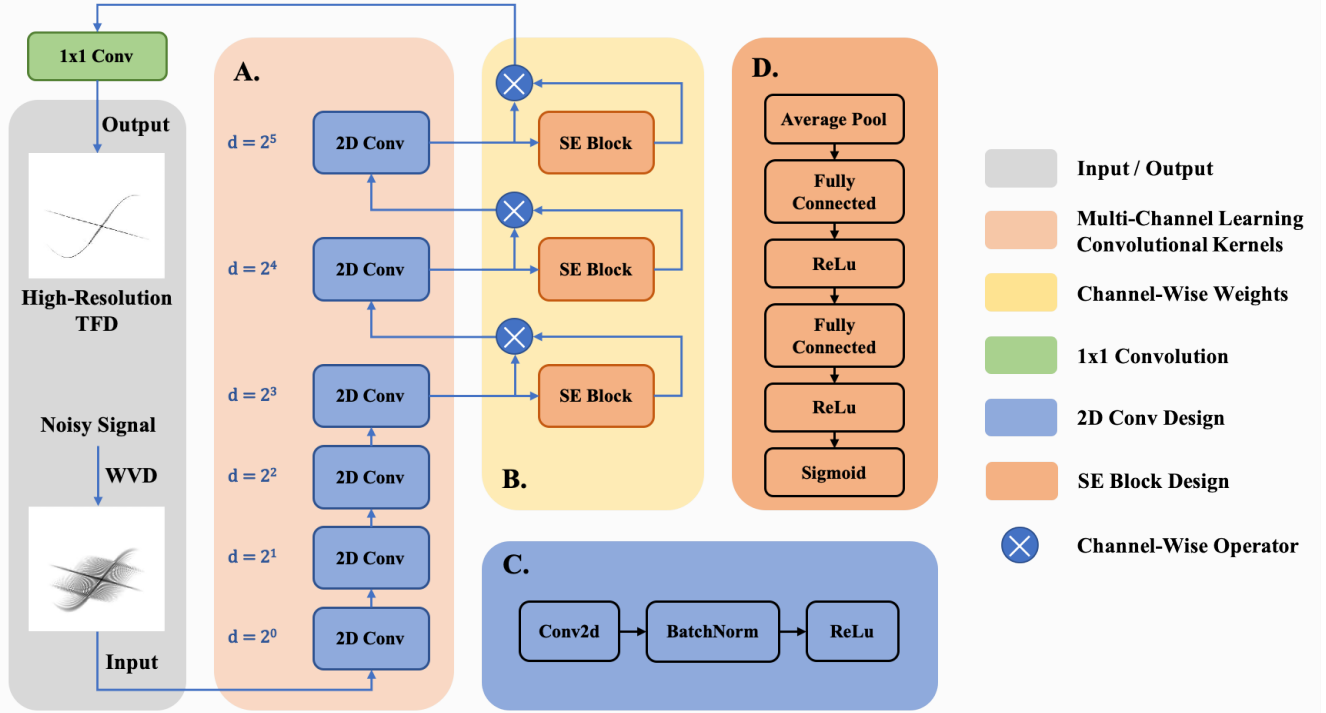


Fig. 1: The block diagram of the proposed KL-TFD. (A) Multi-channel learning module consisting of $K = 6$ 2D Conv blocks with increasing dilation. (B) Channel-wise weight module. (C) 2D Conv design. (D) SE block design.

as low computation. Afterwards, channel-wise weights are gained by squeeze-and-excitation (SE) operations [31], which give rise to better performance. Finally, the 1×1 convolution kernel converts multi-channel into one channel output, i.e., a smoothed WVD (high-resolution TFD) is obtained.

This paper proceeds as follows. Section II elaborates the proposed kernel learning based TFD model. In Section III, the proposed KL-TFD is evaluated by both synthetic as well as real-life signals. Eventually, Section IV concludes this paper.

II. THE PROPOSED KERNEL LEARNING BASED TFD

As shown in Fig. 1, the architecture of the proposed KL-TFD mainly consists of two modules: multi-channel learning convolutional kernels and channel-wise weights. These modules are introduced in detail below.

A. Multi-Channel Learning Convolutional Kernels

For an analytic signal $z(t)$ with N samples, Cohen's class distributions can be interpreted as weighted versions of ambiguity function (AF) smoothed by a low-pass filter $\Phi(\theta, \tau)$. The AF of $z(t)$ is written as:

$$A_z(\theta, \tau) = \int_{-\infty}^{\infty} z\left(t + \frac{\tau}{2}\right) z^*\left(t - \frac{\tau}{2}\right) e^{-j2\pi\theta t} dt. \quad (1)$$

Thus, the general formula of Cohen's class distributions is expressed as [4]:

$$\zeta_z(t, f) = \int_{-\infty}^{\infty} \int_{-\infty}^{\infty} A_z(\theta, \tau) \Phi(\theta, \tau) e^{j2\pi(\theta t - f\tau)} d\theta d\tau, \quad (2)$$

where when $\Phi(\theta, \tau) = 1$, $\zeta_z(t, f)$ is degenerated into WVD, which is defined as 2D Fourier transform of AF, i.e.,

$$W_z(t, f) = \int_{-\infty}^{\infty} z\left(t + \frac{\tau}{2}\right) z^*\left(t - \frac{\tau}{2}\right) e^{-j2\pi f\tau} d\tau. \quad (3)$$

According to convolution theorem, the expression in equation (2) can be rewritten as the form of 2D convolution operation as below [4]:

$$\zeta_z(t, f) = W_z(t, f) ** \gamma(t, f), \quad (4)$$

where $**$ denotes the 2D convolution operator, and $\gamma(t, f)$ is a 2D convolutional kernel which is computed by 2D Fourier transform of AF kernel function $\Phi(\theta, \tau)$.

Additionally, the ADTFD is defined as the 2D convolution of a quadratic TFD with an adaptive directional filter [27]:

$$\zeta_{\text{adapt}}(t, f) = W_z(t, f) ** \gamma_{\beta}(t, f), \quad (5)$$

where $\gamma_{\beta}(t, f)$ denotes the double derivative directional Gaussian filter (DGF), and β is the rotation angle with respect to the time axis. For all the TF points, their angles are selected by optimization among a group of directions at the same time.

Inspired by the 2D convolution relationship in (4) and (5), we propose to employ multi-channel learning convolutional kernels to replace kernel functions or adaptive directional filters, i.e., multi-channel kernels are used to learn different directions at each TF point. As seen in Fig. 1 (A), the signal's WVD serves as the input data, and then K 2D Conv blocks are stacked with increasing dilation, as a result of which fewer parameters can be used while enlarging kernel size, i.e., the receptive field increases with kernel concatenation.

Fig. 1 (C) illustrates the design diagram of a 2D Conv block, which involves a 3×3 kernel followed by batch normalization together with the ReLU function. Thus, nonlinear characteristic is obtained meanwhile overfitting can be avoided to some extent. In particular, each kernel has multiple channels, the number of which ranges from 32 to 64 as the number of layers increases. Compared to traditional adaptive directional filters, our model has less parameters in each kernel and the number of channels greatly increases, implying that more directions can be taken into consideration. In addition, benefitting from a sufficient number of training data, the learning convolutional kernels are inclined to be insensitive to noise.

Generally, the output of the multi-channel learning convolutional kernels with K 2D Conv can be written as:

$$\zeta_{\text{mcl}}^{(K)}(t, f) = W_z(t, f) * * \gamma^{(K)}(t, f), \quad (6)$$

where the learning kernel by our KL-TFD is:

$$\gamma^{(K)}(t, f) = \left(\gamma_{c_1}(t, f) * * \gamma_{c_2}(t, f) \cdots * * \gamma_{c_K}(t, f) \right),$$

where $\gamma_{c_k}(t, f)$ denotes the k th 2D Conv block, and c_k is the number of channels in the k th block. As a result, the output of multi-channel learning module $\zeta_{\text{mcl}}^{(K)}(t, f) \in \mathbb{R}^{c_K \times N \times N}$, i.e., the number of output TFDs is the same as the number of channels in the last 2D Conv block.

B. Channel-Wise Weights

Before the channel fusion, to properly determine the direction of each TF point, channel-wise weights are utilized to weight each channel, i.e., primary directions deserve larger weights while smaller weights are assigned to insignificant directions. The directional filter in ADTFD selects adaptive directions by optimizing the correlation between the directional kernel and the modulus of TFD. In contrast, the data-driven kernel learning model can benefit from sufficient training data and our end-to-end network structure tends to be easier to train. To be specific, we make the choice of adopting the same network architecture as squeeze-and-excitation network [31] to estimate decisive directions, which is illustrated in Fig. 1 (B) and (D). Intuitively, multiple channels are squeezed by average pooling firstly so that channel-level feature can be attained:

$$\rho_K = \mathbf{F}_{sq}(\zeta_{\text{mcl}}^{(K)}) = \frac{1}{N^2} \sum_{i=1}^N \sum_{j=1}^N \zeta_{\text{mcl}}^{(K)}(i, j), \quad (7)$$

where $\rho_K \in \mathbb{R}^{c_K \times 1 \times 1}$ are channel-wise statistics and $\mathbf{F}_{sq}(\cdot)$ represents average pooling.

Next, a gating mechanism extracts correlation information between each channel, and channel-wise weights are then obtained via Sigmoid function:

$$\omega_K = \mathbf{F}_{ex}(\rho_K) = \sigma(g(\rho_K, \mathbf{W})) = \sigma(\mathbf{W}_2 \delta(\mathbf{W}_1 \rho_K)), \quad (8)$$

where $\omega_K \in \mathbb{R}^{c_K \times 1 \times 1}$, $\mathbf{F}_{ex}(\cdot)$ is excitation operation and $g(x, \mathbf{W})$ represents a gating mechanism, which forms a bottleneck with two fully-connected layers around the non-linearity, i.e., the first fully-connected layer $\mathbf{W}_1 \in \mathbb{R}^{\frac{c_K}{r} \times c_K}$ achieves channel reduction with reduction ratio r , then non-linearity

characteristic is introduced by the ReLU function, i.e., δ , and the second fully-connected layer $\mathbf{W}_2 \in \mathbb{R}^{c_K \times \frac{c_K}{r}}$ achieves channel increasing. Finally, channel weights are obtained by Sigmoid function $\sigma = \frac{1}{1 + \exp(-x)}$.

As a result, weighted multi-channel output can be defined as below:

$$\zeta_{\text{wmcl}}^{(K)}(t, f) = \omega_K \otimes \zeta_{\text{mcl}}^{(K)}(t, f), \quad (9)$$

where \otimes denotes the channel-wise operator to realize proper direction selection at each TF point. Thanks to the squeeze-and-excitation operation, channels dependencies can be attained as well which further improves performance. From the viewpoint of parameter reduction, we make the choice of the 1×1 convolution kernel to achieve channel fusion, and the sum of all channels in (9) leads to a smoothed WVD, i.e., a CT-free high-resolution TFD.

III. NUMERICAL EXPERIMENTS

For the parameter setting of the proposed KL-TFD in Fig. 1, the number of 2D Conv blocks in the multi-channel learning module is set to $K = 6$, and the kernel size is 3×3 . The number of channels in the six 2D Conv blocks is respective (32, 64, 64, 64, 64, 64), and corresponding dilation is $(2^0, 2^1, 2^2, 2^3, 2^4, 2^5)$. Channel-wise weight module employs channel reduction $r = (2^2, 2^1, 2^0)$ in three SE blocks respectively. Training datasets are built by synthetic signal mixtures constituted of randomly matched linear frequency-modulated (LFM) and nonlinear sinusoidal frequency-modulated (SFM) components with amplitude modulation (AM) at a fixing SNR = 45 dB. We train the KL-TFD network on the above training dataset for 1500 epochs using NVIDIA GeForce GTX 1080 GPUs with 0.01 learning rate, and the batch size is set to 16. In addition, commonly-used mean square error (MSE) loss function is adopted to obtain a robust network.

Although only trained on synthetic data, our proposed KL-TFD method is validated over synthetic as well as real-life signals, and compared with state-of-the-art kernel design methods [4], [28], including WVD [2], CKD [22], BD [19], MDD [29], AOK [25], RGK [23], and ADTFD [26]¹. The ℓ_1 distance to model and Rényi entropy [5] are regarded as two criteria to quantitatively assess the above-mentioned methods.

A. TFDs of Synthetic Spectrally-Overlapped Signal

We consider synthetic test signal $x(t)$ which can be composed of any two of the following three components:

$$\begin{cases} x_1(t) = a(t) \cos \{2\pi (-0.0003(t^2 - t_0^2) + 0.29(t - t_0))\}, \\ x_2(t) = a(t) \cos \{2\pi (0.0006(t^2 - t_0^2) + 0.109(t - t_0))\}, \\ x_3(t) = a(t) \cos \{0.42\pi(t - t_0) \\ \quad + 31.7 \sin(0.0078\pi(t - t_0) - \phi_0) - 31.7 \sin \phi_0\}, \end{cases}$$

where $a(t) = \exp(0.0078t - 1)^2$ is an Gaussian AM function, t_0 equals to 128, and $\phi_0 = -1.83$.

¹We would like to thank the authors in these works for sharing the source codes of these methods, which are publicly released at <https://github.com/Prof-Boualem-Boashash/TFSAP-7.1-software-package> and <https://github.com/mokhtarmohammadi/Locally-Optimized-ADTFD>.

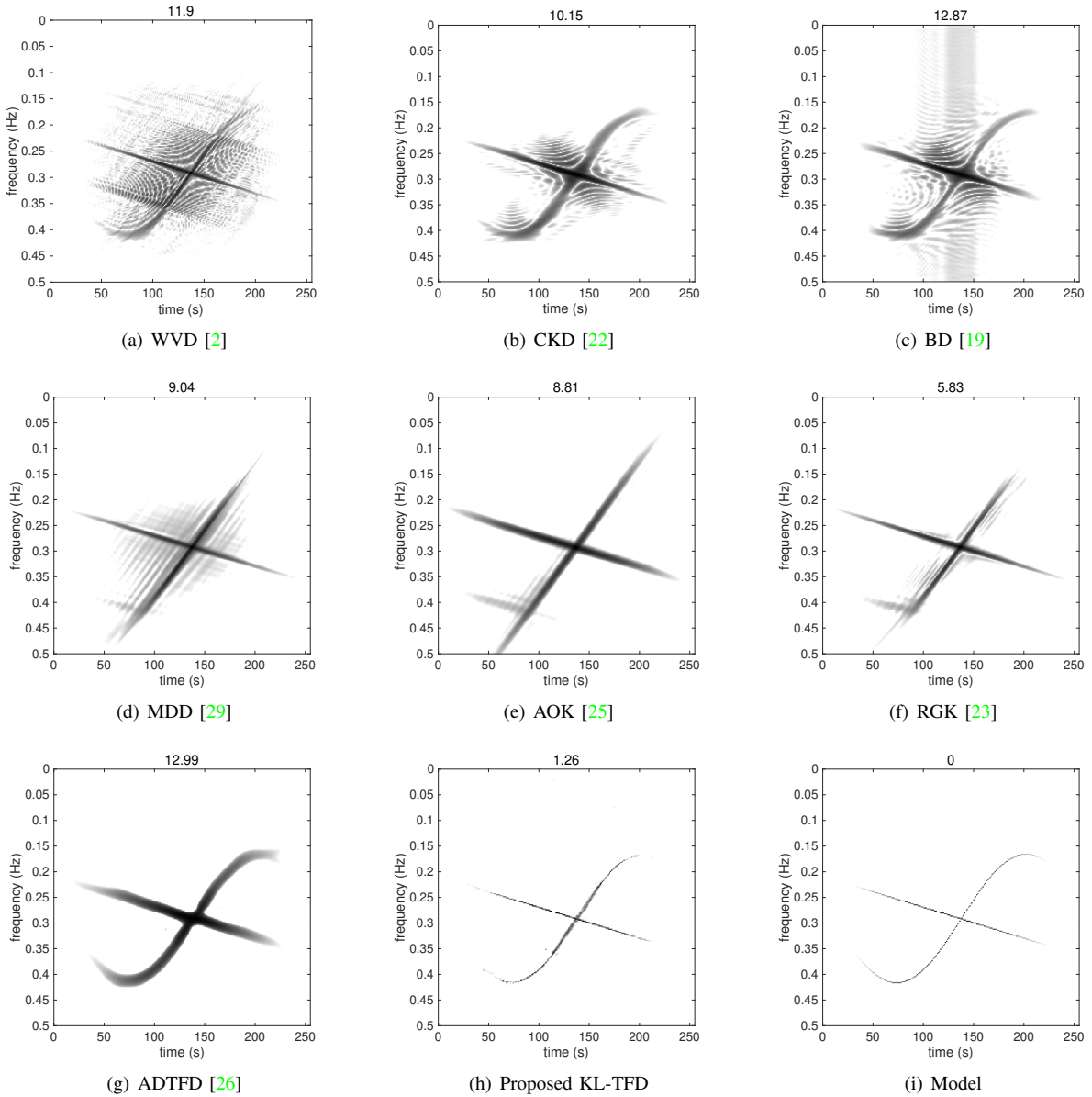


Fig. 2: Generated TFDs of two overlapped AM-LFM and AM-SFM components when SNR = 15 dB using various kernel function based methods: (a) WVD (b) CKD (c) BD (d) MDD (e) AOK (f) RGK (g) ADTFD and (h) the proposed kernel learning based TFD. The ℓ_1 distance to model presented in (i) is annotated on the top of each TFD.

Firstly, the signal $x(t) = x_1(t) + x_2(t)$ including two spectrally-overlapped AM-LFM components with $N = 256$ samples is tested. The evaluation results concerning ℓ_1 distance to model for the overlapped AM-LFM signal using different TFD methods are presented in Table I by changing the SNR level of test data from 45 dB to 0 dB, where 100 trials are implemented at each SNR. Note that even though our training dataset only contains signals at a high SNR = 45 dB, the proposed KL-TFD always achieves a large performance gain compared to other methods especially under low SNR levels, which indicates that the kernel learning model is insensitive to noise benefitting from a large number of training data.

Secondly, the signal $x(t) = x_1(t) + x_3(t)$ including an AM-LFM component and a nonlinear AM-SFM component

TABLE I: The metric values of ℓ_1 distance to model¹ for synthetic overlapped AM-LFM signal at various SNR levels.

SNR	WVD	CKD	AOK	ADTFD	RGK	KL-TFD
45 dB	9.52	10.48	9.05	9.11	6.89	0.79
35 dB	9.62	10.52	9.05	9.10	6.90	0.79
25 dB	10.09	10.70	9.07	9.08	6.91	0.79
15 dB	12.17	11.69	9.28	9.26	7.21	0.81
5 dB	21.94	17.05	11.66	11.21	9.79	1.01
0 dB	37.05	26.66	19.03	15.79	15.84	1.45

¹ The smaller the value is, the closer to the ideal TFD.

is further tested. For visualization of experimental results, Fig. 2 exhibits various TFDs generated by our proposed KL-

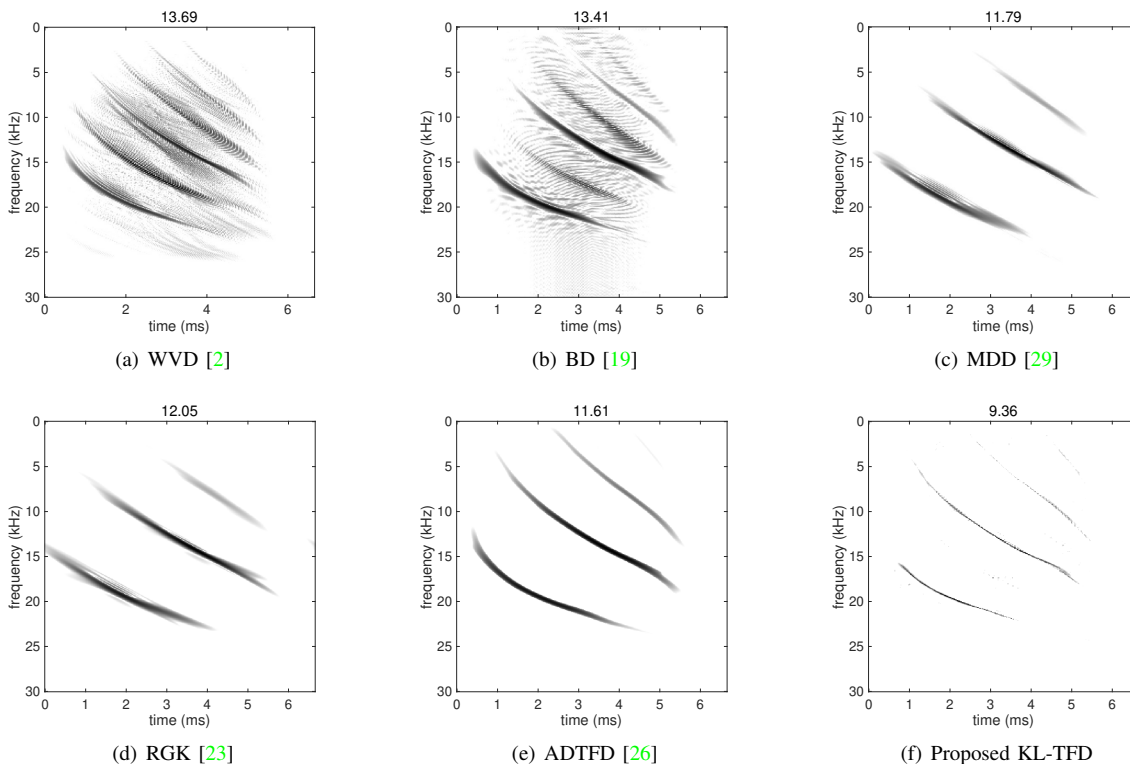


Fig. 3: TFDs of real-life bat echolocation signal when SNR = 20 dB using different kernel design methods: (a) WVD (b) BD (c) MDD (d) RGK (e) ADTFD and (f) the proposed KL-TFD. The Rényi entropy is annotated on the top of each TFD.

TFD method and seven typical kernel function design methods when SNR = 15 dB. It is seen that the WVD is seriously disturbed by both CTs and noise. The CKD and BD can suppress noise to some extent, but at the expense of TF resolution deterioration. In contrast, it is obvious that signal-dependent MDD, AOK, and RGK lead to higher TF resolution while better eliminating CTs, as shown from Fig. 2(d) to Fig. 2(f). Nevertheless, these methods have performance limitation for nonlinear signals. Since the directions of every sample in TFD are taken into consideration, the ADTFD is examined to perform much well with respect to nonlinear signals. As seen from Fig. 2(g), CTs are greatly removed while the nonlinearity of signal's TFD is preserved. However, a trade-off between TF resolution and CTs reduction should be made. Furthermore, the parameters of filter shape and window length are manually selected, i.e., it is a challenging task to obtain ideal performance. Whereas the proposed KL-TFD significantly improves TF resolution, moreover, useless information is largely reduced. From the view of the ℓ_1 distance to model, the KL-TFD achieves 1.26 which is much lower than those achieved by other methods.

B. TFDs of Real-Life Bat Echolocation Signal

Next, we examine the effectiveness of the proposed KL-TFD method compared against WVD, BD, MDD, RGK, and ADTFD on a real-life bat echolocation signal with 400 data points. The evaluation results concerning Rényi entropy for the real-life bat echolocation signal using different TFD methods

TABLE II: The metric values of Rényi entropy² for real-life bat echolocation signal at various SNR levels.

SNR	WVD	BD	MDD	RGK	ADTFD	KL-TFD
45 dB	13.57	13.34	11.73	12.01	11.39	9.27
35 dB	13.57	13.34	11.73	12.01	11.39	9.27
25 dB	13.61	13.35	11.74	12.01	11.40	9.29
15 dB	13.87	13.47	11.84	12.05	11.49	9.42
5 dB	14.85	14.16	12.83	12.48	12.11	9.48
0 dB	15.49	14.92	14.68	13.28	13.00	9.50

² The smaller the value is, the higher the TF resolution is.

are presented in Table II with SNR levels ranging from 45 dB to 0 dB. It indicates that the highest TF resolution is obtained in different noisy environment using our proposed KL-TFD when compared to other methods. The visualized TFD results when SNR = 20 dB using the above six kernel methods are shown in Fig. 3. It is observed that the signal-dependent methods have better performance than signal-independent WVD and BD, i.e., CTs are greatly removed. Obviously, our KL-TFD achieves a large resolution gain compared to others. Experimental results show that our proposed KL-TFD method can break the trade-off between high-resolution and cross-term suppression, which is an issue often encountered by traditional TFD methods.

Finally, we discuss why we choose the training data with a fixing SNR = 45 dB to train our model and the computational complexity of the KL-TFD model. It is analyzed that training

data with various SNR levels may undermine the performance of our model. On the one hand, the energy of strong noise tends to be close to weak-energy components of signals in a low SNR case, resulting in excessive noise suppression, i.e., some useful components with weak energy can be suppressed. On the other hand, overfitting appears when training data are excessive because signals with various noise levels still have extremely similar WVD. To further examine our analysis, we have made an attempt to train our model using training datasets including signals with different SNR levels, and the performance of the KL-TFD deteriorates indeed. As for the computational complexity of the KL-TFD, we then analyze the model size in Fig. 1. Intuitively, the model size is proportional to the number of 2D Conv and SE blocks used in Fig. 1 (A) and (B). Additionally, the computation time also depends on the number of channels in each 2D Conv and the channel reduction r in each SE block. In particular, the number of channels in 2D Conv is related to the parameter size of SE block, which plays a decisive role in model size. Therefore, the channel reduction r makes a balance between model size and model performance.

IV. CONCLUSION

In this paper, we attempt to generate high-resolution TFD by proposing a data-driven kernel learning model, which is designed as an end-to-end network to replace traditional kernel functions, where multi-channel learning kernels and channel-wise weights are two dominant network modules. To be specific, the former module consists of several 2D convolutions stacked with increasing dilation, aiming at obtaining various directions of signals, i.e., each channel is a small directional filter. The latter module is composed of squeezed and excitation operation, leading to weighted multi-channel output. Finally, the 1×1 convolution kernel implements channel fusion, thus attaining a smoothed WVD, i.e., a high-resolution TFD. Experiments on both synthetic and real-life signals verify the effectiveness of the proposed KL-TFD, and demonstrate that supervised kernel parameter learning approaches using neural network based models for high-resolution TFDs outperform their traditional kernel design counterparts.

REFERENCES

- [1] L. Stankovic, M. Dakovic, and T. Thayaparan, "Time-Frequency Signal Analysis With Applications," *Artech House*, 2013.
- [2] B. Boashash, "Time-Frequency Signal Analysis and Processing (Second Edition)," *Academic Press*, 2016.
- [3] P. Flandrin, "Explorations in Time-Frequency Analysis," *Cambridge University Press*, 2018.
- [4] B. Boashash and S. Ouelha, "Designing high-resolution timefrequency and timescale distributions for the analysis and classification of non-stationary signals: a tutorial review with a comparison of features performance," *Digital Signal Processing*, vol. 77, pp. 120 – 152, 2018.
- [5] P. Flandrin and P. Borgnat, "Time-Frequency Energy Distributions Meet Compressed Sensing," *IEEE Trans. Signal Process.*, vol. 58, no. 6, pp. 2974–2982, Jun. 2010.
- [6] H. Zhang, G. Bi, W. Yang, S. G. Razul, and C. M. S. See, "IF estimation of FM signals based on time-frequency image," *IEEE Transactions on Aerospace and Electronic Systems*, vol. 51, no. 1, pp. 326–343, 2015.
- [7] H. Zhang, G. Bi, S. G. Razul, and C. M. S. See, "Robust time-varying filtering and separation of some nonstationary signals in low SNR environments," *Signal Processing*, vol. 106, pp. 141 – 158, 2015.
- [8] E. Sejdić, I. Djurović, and J. Jiang, "Timefrequency feature representation using energy concentration: An overview of recent advances," *Digital Signal Processing*, vol. 19, no. 1, pp. 153 – 183, 2009.
- [9] V. S. Amin, Y. D. Zhang, and B. Himed, "Sparsity-based Time-Frequency Representation of FM Signals With Burst Missing Samples," *Signal Process.*, vol. 155, pp. 25–43, Feb. 2019.
- [10] I. Volaric, V. Sucic, and S. Stankovic, "A Data Driven Compressive Sensing Approach for Time-Frequency Signal Enhancement," *Signal Process.*, vol. 141, pp. 229–239, Dec. 2017.
- [11] I. Daubechies, "The Wavelet Transform, Time-frequency Localization and Signal Analysis," *IEEE Trans. Inf. Theory*, vol. 36, no. 5, pp. 961–1005, Sep. 1990.
- [12] F. Auger and P. Flandrin, "Improving the Readability of Time-Frequency and Time-Scale Representations by the Reassignment Method," *IEEE Trans. Signal Process.*, vol. 43, no. 5, pp. 1068–1089, May 1995.
- [13] S. Wang, X. Chen, G. Cai, and et al., "Matching Demodulation Transform and Synchrosqueezing in Time-Frequency Analysis," *IEEE Trans. Signal Process.*, vol. 62, no. 1, pp. 69–84, 2013.
- [14] T. Oberlin, S. Meignen, and V. Perrier, "Second-Order Synchrosqueezing Transform or Invertible Reassignment? Towards Ideal Time-Frequency Representations," *IEEE Trans. Signal Process.*, vol. 63, no. 5, pp. 1335–1344, 2015.
- [15] G. Yu, M. Yu, and C. Xu, "Synchroextracting Transform," *IEEE Trans. Industrial Electronics*, vol. 64, no. 10, pp. 8042–8054, 2017.
- [16] Abdoush, Y. and Pojani, G. and Corazza, G. E., "Adaptive Instantaneous Frequency Estimation of Multicomponent Signals Based on Linear Time-Frequency Transforms," *IEEE Trans. Signal Process.*, vol. 67, no. 12, pp. 3100–3112, 2019.
- [17] F. Hlawatsch and G. F. Boudreaux-Bartels, "Linear and quadratic time-frequency signal representations," *IEEE Signal Processing Magazine*, vol. 9, no. 2, pp. 21–67, 1992.
- [18] H. I. Choi and W. J. Williams, "Improved Time-Frequency Representation of Multicomponent Signals Using Exponential Kernels," *IEEE Transactions on Acoustics, Speech, and Signal Processing*, vol. 37, no. 6, pp. 862–871, Jun. 1989.
- [19] B. Barkat and B. Boashash, "A High-Resolution Quadratic Time-Frequency Distribution for Multicomponent Signals Analysis," *IEEE Trans. Signal Process.*, vol. 49, no. 10, pp. 2232–2239, Oct. 2001.
- [20] L. Stankovic, "A Method for Time-Frequency Analysis," *IEEE Trans. Signal Process.*, vol. 42, no. 1, pp. 225–229, Jan. 1994.
- [21] B. Boashash, G. Azemi, and J. M. O'Toole, "Time-Frequency Processing of Nonstationary Signals: Advanced TFD Design to Aid Diagnosis with Highlights From Medical Applications," *IEEE Signal Process. Mag.*, vol. 30, no. 6, pp. 108–119, Nov. 2013.
- [22] M. Abed, A. Belouchrani, M. Cheriet, and B. Boashash, "Time-frequency distributions based on compact support kernels: Properties and performance evaluation," *IEEE Transactions on Signal Processing*, vol. 60, no. 6, pp. 2814–2827, 2012.
- [23] R. G. Baraniuk and D. L. Jones, "Signal-dependent Time-Frequency Analysis Using a Radially Gaussian Kernel," *Signal Process.*, vol. 32, no. 3, pp. 263–284, Jun. 1993.
- [24] D. L. Jones and R. G. Baraniuk, "An Adaptive Optimal-Kernel Time-Frequency Representation," in *Int. Conf. Digital Signal Process.*, vol. 4, USA, 1993, pp. 109–112.
- [25] D. L. Jones and R. G. Baraniuk, "An adaptive optimal-kernel time-frequency representation," *IEEE Trans. Signal Process.*, vol. 43, no. 10, pp. 2361–2371, 1995.
- [26] N. A. Khan and B. Boashash, "Multi-Component Instantaneous Frequency Estimation Using Locally Adaptive Directional Time Frequency Distributions," *International Journal of Adaptive Control and Signal Processing*, vol. 30, no. 3, pp. 429–442, 2016.
- [27] N. Ali Khan and S. Ali, "Sparsity-aware adaptive directional time-frequency distribution for source localization," *Circuits Syst. Signal Process.*, vol. 37, no. 3, p. 12231242, Mar. 2018.
- [28] M. Mohammadi, A. A. Pouyan, N. A. Khan, and et al., "Locally Optimized Adaptive Directional Time-Frequency Distributions," *Circuits, Systems, and Signal Processing*, vol. 37, no. 8, pp. 3154–3174, 2018.
- [29] B. Boashash and S. Ouelha, "An Improved Design of High-Resolution Quadratic Time-Frequency Distributions for the Analysis of Nonstationary Multicomponent Signals Using Directional Compact Kernels," *IEEE Trans. Signal Process.*, vol. 65, no. 10, pp. 2701–2713, May 2017.
- [30] L. Jiang, H. Zhang, and L. Yu, "Robust Time-Frequency Reconstruction by Learning Structured Sparsity," arXiv:2004.14820, 2020.
- [31] J. Hu, L. Shen, and G. Sun, "Squeeze-and-Excitation Networks," in *Proceedings of the IEEE conference on computer vision and pattern recognition*, 2018, pp. 7132–7141.